Engineering 2015, 1(3): 309–323
DOI 10.15302/J-ENG-2015082

Research
Medical Instrumentation—Review

Optical Molecular Imaging Frontiers in Oncology: The Pursuit of Accuracy and Sensitivity

Kun Wang[#], Chongwei Chi[#], Zhenhua Hu[#], Muhan Liu, Hui Hui, Wenting Shang, Dong Peng, Shuang Zhang, Jinzuo Ye, Haixiao Liu, Jie Tian*

ABSTRACT Cutting-edge technologies in optical molecular imaging have ushered in new frontiers in cancer research, clinical translation, and medical practice, as evidenced by recent advances in optical multimodality imaging, Cerenkov luminescence imaging (CLI), and optical image-guided surgeries. New abilities allow *in vivo* cancer imaging with sensitivity and accuracy that are unprecedented in conventional imaging approaches. The visualization of cellular and molecular behaviors and events within tumors in living subjects is improving our deeper understanding of tumors at a systems level. These advances are being rapidly used to acquire tumor-to-tumor molecular heterogeneity, both dynamically and quantitatively, as well as to achieve more effective therapeutic interventions with the assistance of real-time imaging. In the era of molecular imaging, optical technologies hold great promise to facilitate the development of highly sensitive cancer diagnoses as well as personalized patient treatment—one of the ultimate goals of precision medicine.

KEYWORDS optical molecular imaging, multimodality molecular imaging, optical multimodality tomography, Cerenkov luminescence imaging, intraoperative image-guided surgery

1 Introduction

Imaging has become an unprecedentedly powerful tool in preclinical cancer research and clinical practice. In the past 15 years, there has been a significant increase in the number of imaging technologies and their applications in the field of oncology [1–4], but perhaps the biggest breakthroughs are in the new developments in optical molecular imaging (OMI). With recent advances in optical multimodality imaging, Cerenkov luminescence imaging (CLI), and intraoperative optical image-guided surgery, the sensitivity and accuracy of tumor diagnoses and therapeutic interventions have moved to a whole new level. Researchers and clinicians are now on the verge of being able to address some of the important questions in oncology that were once impossible to conclusively answer. How do we shift from conventional *in vitro* assay-based findings to non-invasive *in vivo* imaging-based detection? Is it possible to obtain accurate and quantitative biological information (e.g., the receptor density in tumor tissues) on a three-dimensional (3D) cellular or sub-cellular level? How can we better delineate tumor boundaries and guide tumor resection? Can we exceed the sensitivity limitation of conventional imaging methods for effective small tumor foci detection both preoperatively and intraoperatively? How do we translate preclinical OMI into clinical applications for better tumor treatment outcomes?

In this article, we highlight some recent advances of OMI in three categories: optical multimodality imaging, CLI, and optical image-guided surgery. We review cutting-edge optical imaging instruments, the development of optical tomographic imaging models and reconstruction algorithms, and promising optical imaging strategies with smart utilization of multiple molecular probes in both breadth and depth. We also demonstrate specific applications and state-of-the-art *in vivo* imaging examples of OMI in biomedical research and recent clinical translations.

2 *In vivo* optical multimodality molecular imaging

Different imaging modalities have their inherent advantages and disadvantages, and they are complementary. For example, radionuclide imaging has a superb sensitivity to molecular targets but a limited spatial resolution, whereas computed tomography (CT) and magnetic resonance imaging (MRI) can offer good spatial resolution but suffer from low sensitivity in detecting molecular events [5]. Planar optical imaging that adopts photographic principles is the simplest technique for capturing visible and/or near-infrared (NIR) light emitting from optical reporter molecules *in vivo* [6–8]. This planar

Key Laboratory of Molecular Imaging, Institute of Automation, Chinese Academy of Sciences, Beijing 100190, China
[#] Parallel first authors
* Correspondence author. E-mail: tian@ieee.org
Received 6 August 2015; received in revised form 6 September 2015; accepted 10 September 2015

technique can offer good superficial resolution (the resolution of an imaging subject surface), high sensitivity, and high-throughput imaging ability, and it is technically easy to implement preclinically [9]. However, it also has two major limitations. The first limitation is the difficulty in quantification of the *in vivo* distribution of optical probes due to the nonlinear relationship in spatial position and signal strength between the detected surface flux and the light source [10]. The second is the relatively shallow imaging depth due to the significant light scattering and absorption inside the tissue and organs of imaged animals [11]. These features result in the application of this approach primarily to qualitative superficial observation. Although various efforts have been made to develop different algorithms for tomographic reconstruction solely using planar optical images, the process inevitably involves erroneous interpretation of the data collected unless the nonlinear effects are explicitly corrected or accounted for [9]. Therefore, combining planar optical imaging with other modalities is recommended in order to compensate for these limitations while building on its strengths to capitalize on its great potential [12].

2.1 From 2D qualitative to 3D quantitative imaging

Tomographic reconstruction of the biodistribution of optical molecular probes can be traced back to the early 1990s. The first theoretical frameworks were proposed as a way to spatially resolve intrinsic tissue contrast in the context of studying hemodynamics or organelle concentration [13–16]. Visible and NIR photons (from 650 nm to 950 nm) are highly scattered in tissue and start to diffuse within a millimeter of propagation [17]. However, a portion of the light can still penetrate several centimeters and reach a small-animal skin surface because of the low photon absorption in this spectral window [18, 19], which is known as the first NIR window (NIR-I) [20, 21]. At wavelengths shorter than 650 nm, there is an increased absorption by blood (oxygenated and deoxygenated) and skin, whereas at wavelengths longer than 950 nm, water and lipids demonstrate stronger absorption.

In recent optical multimodality tomography (OMT), the diffuse light patterns are collected from a small animal surface at one or multiple angles using photodetector sets or various charge-coupled-device (CCD) cameras. Meanwhile, the anatomical structure of the animal is acquired using CT or MRI (Figure 1) as one of the *a priori* sets of information for helping optical reconstruction. Based on the types of optical molecular probe applied, this 3D non-invasive whole-body small-animal imaging technology is subdivided into three categories: fluorescence molecular tomography (FMT, employing fluorescent probes and external illumination sources) [22, 23], bioluminescence tomography (BLT, employing reporter genes, luciferin substrates, and no external illumination sources) [24, 25], and Cerenkov luminescence tomography (CLT, employing radioactive probes and no external illumination sources) [26, 27]. With the presence of the extra dimension, the combination of sufficient imaging information from different modalities, and appropriate optical molecular probes with specificity to cellular and sub-cellular processes, OMT is able to overcome the first limitation of the conventional planar optical imaging technique mentioned earlier, and offer more accurate and robust quantitative imaging on a cellular and molecular level.

The hardware setup of these multimodality imaging methods may vary in different biomedical applications or when prepared by different research groups (Figure 1). Examples include the hybrid optical-CT imaging system shown in Figure 1(a) and (b), the hybrid optical-MRI system in Figure 1(c)–(e), and the triple-modality optical-CT-MRI system shown in Figure 1(f) and (g). However, there are two generic factors that have significant influence on tomographic performance. First, it is crucial to develop appropriate mathematical imaging models describing photon propagation in tissues—an issue that is known as the forward problem; and second, it is equally important to develop sophisticated algorithms for tomographic reconstruc-

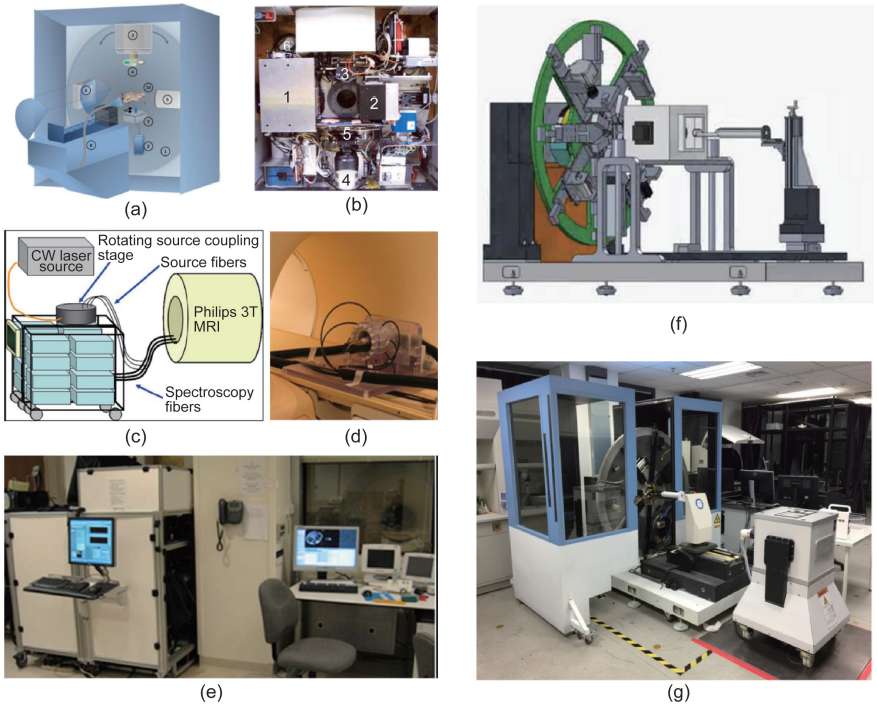

Figure 1. Examples of different OMT systems. (a) The diagram and (b) internal structure of the hybrid FMT-CT system developed by the Vasilis Ntziachristos group, reproduced from Refs. [28, 29]; the optical and CT subsystems are perpendicular to each other, and the mouse lies in the center of the rotating gantry during imaging acquisition. (c)–(e) The FMT-MRI system developed by the Brian Pogue group, reproduced from Ref. [30]. (c) A diagram of the MRI-coupled 16-channel optical system for fluorescence tomography. (d) The mouse with MRI coil and fiber bundles lies inside a clinical 3T MRI system. (e) The optical system is inside the MRI control room. (f) & (g) The triple-modality optical-CT-MRI system developed by the Jie Tian group. (f) The system design diagram shows that the optical and CT subsystems are installed on the rotating gantry, whereas the cubic MRI subsystem (1 T permanent magnet) is installed in the middle of the gantry and the small animal transmit unit. Since the system is still in development, the final position of the MRI subsystem may differ from the original design (g).

tion—an issue that is known as the inverse problem [9, 10].

Typical forward problems proposed for OMT are based on numerical or analytical solutions of the diffusion equation with the assumption that the imaging subjects are homogeneous in optical properties [31–33]. To further improve the accuracy, different forward models based on approximate solutions to the radiative transport equation, on diffusion equation solutions merged with radiosity principles, or on higher-order spherical harmonic approximations were also proposed for different tissue and organs where optical properties were assumed to be heterogeneous inside living small animals [10, 34, 35]. There is an evolution of the optical imaging model toward better accuracy with acceptable increase of the computational cost for *in vivo* applications.

Due to high photon scattering in tissues, the system matrix of OMT is ill-conditioned and the inverse reconstruction is ill-posed [36]. In contrast to single modality optical tomography, OMT can utilize prior information or guidance obtained from other imaging modalities in order to minimize these problems. Furthermore, various regularization methods, such as Tikhonov regularization [37], sparsity regularization [38], total variation regularization [39], and reweighted L_2 and L_1 regularizations [40, 41], can be employed to achieve computationally fast and robust reconstruction. These methods can be used with fast analytical solvers or numerical solutions in order to further accelerate the reconstruction speed [42, 43]. Overall, there is a consistent demand for faster and more robust inverse algorithms, as the acquired data sets increase in size due to the application of more complicated multimodality imaging systems.

With the rapid development of hardware systems, optical imaging models, and tomographic reconstruction algorithms, OMT has become more and more practical and easy to implement. In the last decade, there has been a significant shift from mathematical simulation or artificial phantom studies to *in vivo* small-animal studies in the field of OMT. A wide range of unique biomedical applications in small-animal tumor model imaging was investigated by several pioneering groups all over the world. Here, we summarize some of the most recent breakthrough studies in order to demonstrate the superiority of the hybrid FMT and BLT. As CLT is reviewed in more detail in Section 3, we do not introduce its *in vivo* applications in this section in order to avoid repetition.

The Vasilis Ntziachristos group has successfully achieved highly accurate hybrid FMT-CT performance on a subcutaneous 4T1 tumor mouse model, an Aga2 osteogenesis imperfecta model, a Kras lung cancer mouse model and a pancreatic ductal adenocarcinoma model, as shown in Figure 2(a) [28, 29]. The *in vivo* imaging results were compared to single modal FMT and CT, respectively, and were also validated against

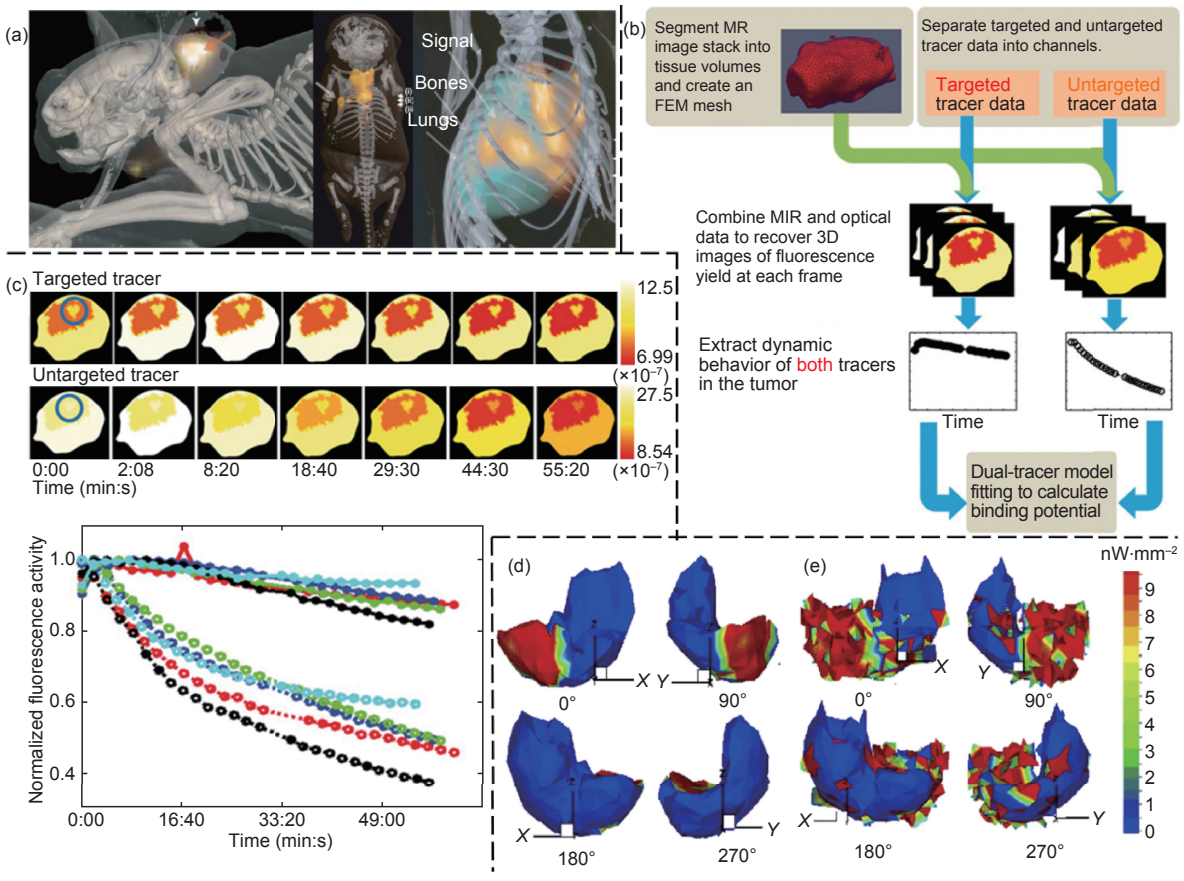

Figure 2. The non-invasive *in vivo* application of OMT. (a) 3D reconstruction of a subcutaneous 4T1 tumor model, an Aga2 osteogenesis imperfecta model, and a Kras lung cancer model using the FMT-CT technique, reproduced from Ref. [28]. (b) A procedure for recovering binding potential using a dynamic dual-tracer FMT-MRI technique, reproduced from Ref. [44]. (c) Dynamic dual-tracer FMT-MRI imaging of gliomas in mice; the first two rows are the time series coronal images showing fluorescence activity of the targeted and untargeted tracers, and the bottom plot shows the time series of fluorescence activity of targeted (● solid lines) and untargeted (○ dotted lines) tracers in the tumors of all animals, clearly demonstrating two different profiles; reproduced from Ref. [44]. Mouse liver reconstruction results of (d) a new designed anti-tumor drug or (e) saline-treated mice using the BLT-CT technique; the images demonstrate that the drug showed higher anti-tumor efficacy compared with the control saline-treatment group. Reproduced from Ref. [45].

post-mortem planar fluorescence images of cryoslices and histology data. The study vividly demonstrated that OMT can provide much more accurate 3D information on tumor lesions than either stand-alone FMT or CT can achieve, or than can be obtained using the planar optical imaging method.

The Jing Bai group and the Brian Pogue group have separately developed FMT-CT and FMT-MRI techniques for dynamic fluorescence molecular imaging, both of which are powerful new four-dimensional tools for cancer research. They are especially useful as better ways of studying receptor-targeted drug delivery and cancer progression non-invasively. These groups employed their OMT approaches and successfully reported the binding kinetics of different optical molecular probes in the blood pool and in tumor xenografts [46–49]. Furthermore, the Brian Pogue group applied this technique to image the uptake kinetics of two optical probes in U251 brain tumor mouse models simultaneously. One probe targeted the receptor of interest, and the other acted as a non-targeted reference. (See Figure 2(b) and (c) for more detail.) These dynamic data were then fit to a dual-tracer compartmental model in order to achieve accurate quantification of the receptor density available for binding therapeutic drugs in tumor tissues [44]. The Pogue group also applied a similar imaging technique with dual-optical probes for the accurate quantification of tumor burden in lymph nodes in breast cancer mouse models. This non-invasive imaging method reached an ultimate sensitivity of approximately 200 cells in detecting breast cancer metastasis (potentially more sensitive than conventional lymph node biopsy) [50].

In contrast to the above studies, the Jie Tian group developed a BLT-CT technique that was sufficient for *in vivo* imaging and applied it to evaluate the therapeutic interventions of new designed anti-tumor drugs [45, 51]. For *in vivo* planar bioluminescence imaging (BLI) or 3D BLT, biological entities (e.g., tumor cells, immune cells, bacteria, or genes) are tagged with a reporter gene that encodes one of a number of light-generating enzymes (luciferases). In the presence of oxygen and other factors (e.g., ATP, Mg), enzymes convert unique substrates (luciferin) into light [52–54]. The propagation of emitted photons in living animals can be simulated as a diffusion process that is similar to fluorescence photon propagation. However, it is more difficult to achieve practical *in vivo* imaging using BLT than using multimodality FMT approaches, because BLT does not use external illumination sources. Although this feature carries the major advantage of a high tumor-to-normal-tissue contrast due to the absence of inherent background noise, the fewer source-detector pairs available complicate the tomographic problem mathematically.

By integrating multi-angle (from 0° to 360°) imaging with *a priori* information on much more accurately defined tissue heterogeneity, the Jie Tian group improved the performance of the inverse problem of BLT [10]. Their recent studies demonstrate that with well-developed reconstruction algorithms, the technique can provide accurate 3D information on orthotopic liver tumors, and the anti-tumor efficacy of newly developed therapeutic drugs or other interventions can be monitored quantitatively without sacrificing the tumor-bearing mice, as shown in Figure 2(d) and (e) [45, 51].

2.2 Toward deeper imaging depth

In addition to all the technological developments and biomedical applications of OMT described above, other research groups are acquiring optical molecular images and images from other modalities using separate systems, and then combining the information to obtain better sensitivity and accuracy. This optical multimodality molecular imaging strategy normally involves the application of multimodal molecular probes and avoids the difficulty of developing complicated hybrid imaging systems. Recent achievements even circumvented the second limitation of conventional planar optical imaging and achieved deeper imaging depth.

The Sanjiv S. Gambhir group designed a unique triple-modality (MRI-photoacoustic-Raman) imaging nanoprobe [55]. Because of the better tissue-penetrating ability of photoacoustic imaging (PAI) and the better spatial resolution of optical Raman imaging, this triple-modality imaging strategy allowed for non-invasive accurate brain tumor delineation through an intact skull, shown in Figure 3(a) and (b), and even more accurate intraoperative image guidance (micrometer scale) for tumor resection, shown in Figure 3(c)–(e). With the group's in-house-modified imaging systems, the probes were detectable with at least picomolar sensitivity in living mice. These impressive features of this optical multimodality approach hold great promise for enabling more accurate and sensitive brain tumor imaging and resection than ever before.

In Gambhir's study, PAI is the key to overcoming the limitation in optical imaging depth. The reason why this emerging hybrid imaging technique achieves better tissue penetration than conventional fluorescence and bioluminescence imaging is because of its unique utilization of the photoacoustic effect [56]. It employs a pulsed nanosecond-long laser beam instead of a continuous wave to illuminate the targets of interest (biomolecules or molecular probes), causing a slightly localized heating and resulting in thermoelastic expansion. This transient thermoelastic tissue expansion generates pressure waves with high frequency that can be detected by ultrasonic transducers [57]. Therefore, PAI combines the advantages of optical excitation and acoustic detection. Since an acoustic wave has a much lower scattering coefficient in biological tissue than light does, PAI offers imaging at a greater depth than conventional optical imaging methods, as shown in Figure 3(a) and (b), thereby ultrasonically breaking through the optical diffusion limit [58]. Recent advances in PAI have made it a powerful imaging tool in both biological and clinical applications. In recent years, the Lihong Wang group and the Vasilis Ntziachristos group have been developing various PAI instruments and extending the applications of such instruments, respectively [59, 60]. Their efforts are likely to accelerate OMI from preclinical studies toward clinical translations in cancer diagnoses (e.g., the diagnosis of breast carcinoma and skin neoplasm).

In addition to PAI, techniques using the second NIR window (NIR-II, 1000–1400 nm) have also been developed in order to overcome the limitation in optical imaging depth. Compared with the first NIR window, NIR-II can offer deep penetration depth in tissues (reduced scattering effect) and

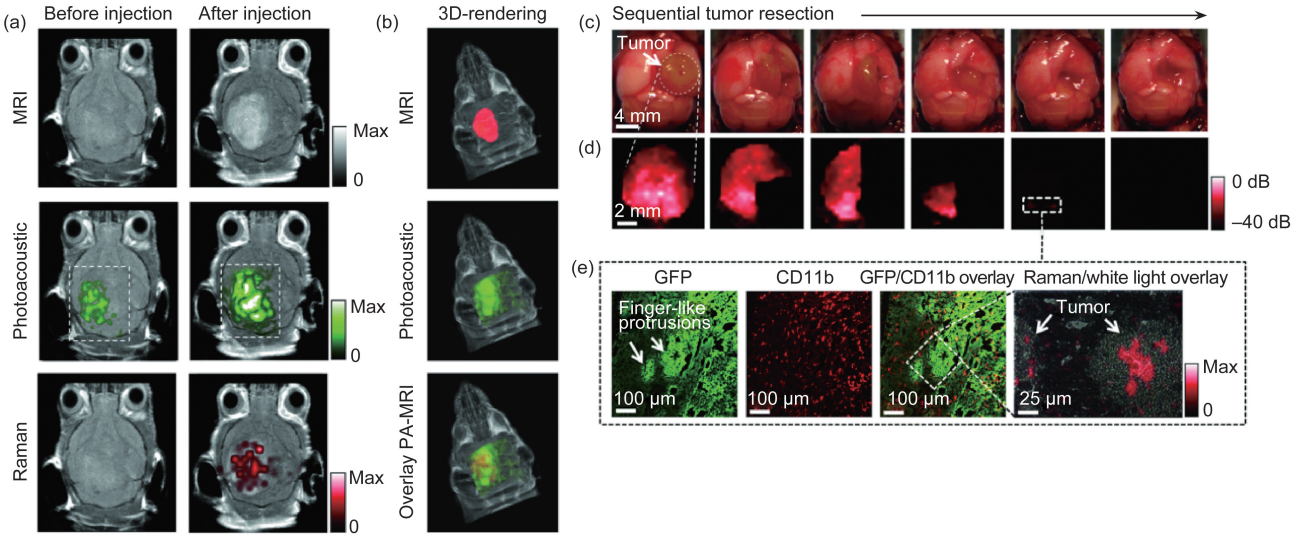

Figure 3. *In vivo* triple-modality detection of brain tumors and Raman-guided intraoperative surgery. (a) After injecting the triple-modality molecular probe, 2D images of all three modalities (MRI, photoacoustic, and Raman) demonstrated clear tumor visualization. (b) 3D-rendering of MR images with the tumor segmented (red; top); overlay of 3D photoacoustic images (green) over MRI (middle); and overlay of MRI segmented tumor and photoacoustic image (bottom). (c) A living tumor-bearing mouse underwent craniotomy under general anesthesia. Quarters of the tumor were then sequentially removed. (d) Intraoperative Raman imaging was performed after each resection step, until the entire tumor had been removed by visual inspection. After the gross removal of the tumor, several small Raman signal foci were found in the resection bed (outlined by the dashed white square). (e) Subsequent histological analysis of sections from these foci demonstrated an infiltrative pattern of the tumor in this location, forming finger-like protrusions extending into the surrounding brain tissue. As shown in the Raman microscopy image (far right), a Raman signal was observed within these protrusions. Reproduced from Ref. [55].

a higher signal-to-noise ratio (low tissue auto-fluorescence) for fluorescence imaging [20]. However, the synthesis of biocompatible and bright NIR-II fluorescent probes and the application of suitable CCD cameras with high quantum efficiency in this longer wavelength window play critical roles for achieving practical *in vivo* NIR-II imaging. The Hongjie Dai group reported the use of biocompatible, bright single-walled carbon nanotubes (SWNTs) as NIR-II imaging contrast agents for the imaging of blood velocity in both normal and ischemic femoral arteries [61]. In this study, an indium gallium arsenide (InGaAs) camera and a conventional silicon (Si) camera were applied for NIR-II and NIR-I imaging, respectively, in a hybrid optical imaging system, as shown in Figure 4(a). A thorough comparison of the imaging performances in the two NIR windows demonstrated the superiority of NIR-II in obtaining more information from deeper tissues, as shown in Figure 4(b) and (c). The group also performed imaging of mouse arterial blood flow in deep tissue at the ultrafast video-rate of > 25 fps (frames per second), with a high quantum yield of synthesized polymers as fluorescent agents, as shown in Figure 4(d)–(f) [62]. Furthermore, Dai's group has reported the non-invasive through-scalp and through-skull brain imaging of mouse cerebral vasculature, without using craniotomy or skull-thinning techniques, as shown in Figure 4(g)–(i) [63]. In this work, the

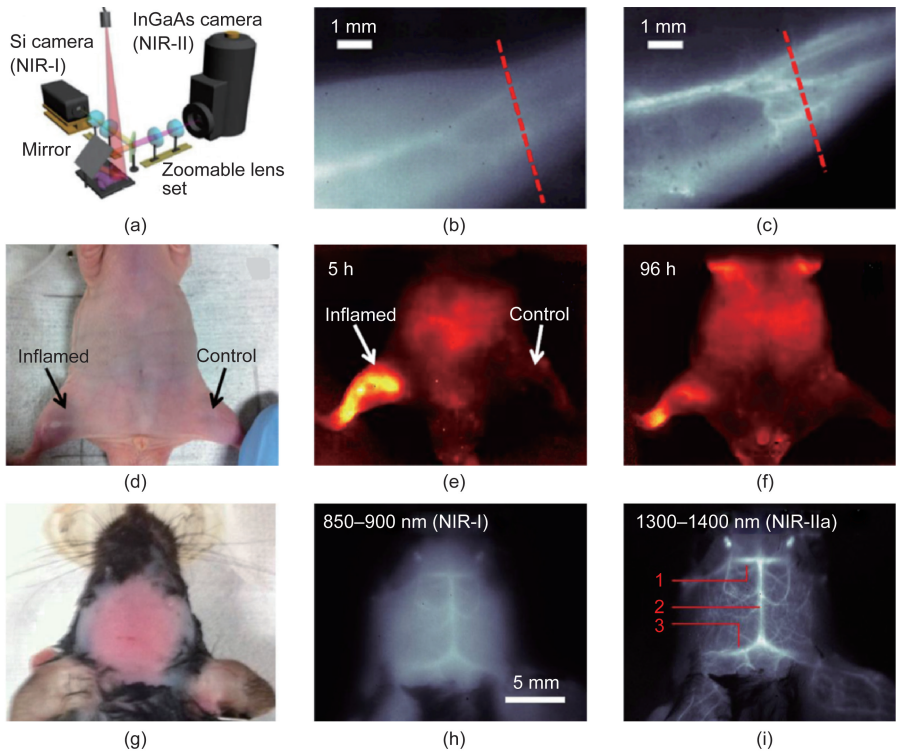

Figure 4. (a) Schematic of the imaging setup for concurrent NIR-I and NIR-II photons using Si and InGaAs cameras. (b) NIR-I fluorescence images and (c) NIR-II fluorescence images of blood vessels in the mouse. (a)–(c) are reproduced from Ref. [61]. (d) Imaging local blood redistribution with pDA-PEG; a white-light image showing the mouse with ~ 5 h heat-induced inflammation in the right hind limb (left to the viewer). (e) & (f) NIR-II fluorescence images of the mouse at different times after inducing inflammation. (d)–(f) are reproduced from Ref. [62]. (g) *In vivo* mouse brain imaging with SWNT-IRDye800 in different NIR subregions. (h) & (i) The same mouse head is imaged both in NIR-I (850–900 nm) and NIR-II (1300–1400 nm) regions. The inferior cerebral vein, the superior sagittal sinus, and the transverse sinus are labeled 1, 2, and 3, respectively in (i). (g)–(i) are reproduced from Ref. [63].

imaging depth was 2 mm deeper than in previous efforts and the imaging rate of 5.3 fps permitted the dynamic monitoring of blood perfusion in the cerebral vessels of the mouse brain.

Recent advances in optical multimodality molecular imaging are embodied in every aspect of the technology, including optical molecular probes, and especially in the nanoscale. An enormous development has occurred in the form of a variety of new nanomaterials that are modified for *in vivo* OMI, such as polymers [64, 65], liposomes, micelles [66], metallic nanoparticles (gold, silver, titanium, and quantum-dot) [67–69], inorganic particles (up- and down-conversion) [70–72], and carbon structures (nanotubes and nanodiamonds) [73, 74]. Many groups are dedicated to synthesizing molecular probes with better optical properties that are applicable for multi-targets as well as for multimodality imaging in order to enhance the overall sensitivity and accuracy of the imaging performance. However, even though there have been significant achievements in preclinical applications with nanoprobes (e.g., ultrasensitive primary gastric tumor and lymphatic metastasis imaging [72], ultrasensitive multiplexed diagnostics [69], etc.), and the future of OMI-based nanotechnology seems promising, the progress of clinical translation in OMI-based nanotechnology has still been slower than expected over the last decade. Major concerns regarding the metabolic rate and toxicity of nanoscale imaging agents inside human systems are still preventing their application in clinical practice. To the best of our knowledge, Doxils, Abraxanes, and Feridexs are the only three nanoscale imaging agents that have been approved by the Food and Drug Administration (FDA) for clinical use. All three are composed of simple formulations without tumor specificity. However, the emergence of CLI and intraoperative fluorescence image-guided surgery may facilitate the clinical translation of OMI with clinically approved radioactive probes and operating-room-fitted imaging systems.

3 Cerenkov luminescence imaging (CLI)

Cerenkov luminescence (CL) is the light generated when charged particles—usually electrons or positrons emitted from radioisotopes upon radioactive decay—exceed the speed of light in a dielectric medium. As an emerging OMI technology, CLI was first reported much more recently than fluorescence and bioluminescence planar or tomographic imaging technologies. Compared with nuclear imaging, which also employs radioactive tracers, CLI has several advantages that are inherent in optical imaging: higher throughput, cost savings, and greater surface resolution [75]. Furthermore, a variety of tracers approved by the FDA enable clinical applications [76–79], giving CLI a unique inborn advantage in clinical translation. However, the low intensity of CL and its violet-blue-dominated spectrum limit its depth of tissue penetration. Hence, significant signal amplification and alternative imaging techniques are required to enhance CLI sensitivity.

CLI suffers from tissue depth-dependent signal weakening, strict restriction of background light, and a lack of additional information, compared with positron emission tomography (PET). To enhance the intensity of CLI signals and to complement PET, radiopharmaceutical-excited fluorescence imaging (REFI) [80], secondary Cerenkov-induced fluorescence imaging (SCIFI) [75], Cerenkov radiance energy transfer (CRET) [81–86], radioluminescence imaging (RLI) [87–91], radioisotope energy transfer (RET) [92], and enhanced CLI (ECLI) [93, 94] have been explored.

Self-illuminating ^{64}Cu-doped nanoparticles (NPs), such as gold nanocages [89], nanoclusters [84, 92], CdSe/ZnS [83, 93], and CuInS/ZnS QD [83], shift Cerenkov radiation toward longer wavelengths. Rare earth nanophosphors doped with Eu^{3+}, Tb^{3+}, Er^{3+}, and Yb^{3+} enable inherent multimodality and increase the signal-to-noise ratio of optical imaging [87, 88, 90, 92, 94]. Among these studies, the Jie Tian group utilized europium oxide nanoparticles and radioactive tracers in order to convert γ and Cerenkov radiation into signal-enhanced red emission [80]. This unique internal dual-radiation excitation mechanism combined the advantages of nuclear and OMI and provided non-invasive yet highly sensitive detection of tiny early-tumor lesions (Figure 5).

In 2010, Liu et al. demonstrated multispectral, deep-tissue, and potentially targeted imaging by the *in vivo* excitation of quantum dots contained in Matrigel pseudotumors using a radiotracer source [82]. The three quantum dots can be multiplexed using corresponding filters in order to acquire information for each channel. In 2013, Thorek et al. proposed SCIFI [75] as a new CL imaging strategy that enables activatable imaging via the biologically specific fluorescent conversion of Cerenkov radiance. The multiparameter imaging of tumor markers with a high signal-to-background ratio is shown by using HER2/neu-targeted ^{89}Zr-DFO-trastuzumab to excite $\alpha_v\beta_3$-targeted cRGD-QD605. The SCIFI signal indicates the co-expression of HER2/neu and $\alpha_v\beta_3$ signatures of tumor cells. Matrix metallopeptidase-2 (MMP-2) enzymatic activity *in vivo* imaging is presented via gold nanoparticles (AuNPs) conjugated with carboxyfluorescein (FAM)-labeled peptides. The peptide sequence IPVSLRSG can be cleaved specifically in the microenvironment of an MMP-2 positive tumor. Specific cleavage of the peptide dissociates fluorescence-quenching AuNPs from FAM; hence, the SCIFI signal indicates MMP-2 enzymatic activity *in vivo*, which correlates with the *ex vivo* quantitative Western blotting assay.

Since Robertson et al. first detected luminescent signals from positron-emitting radionuclides using Xenogen IVIS (IVIS 100 or 200, Caliper Life Sciences, Alameda, CA, USA) [95], CLI featured as a low-cost imaging technology among radionuclide imaging modalities. To break the limit on penetration depth due to the strong scattering of Cerenkov light and to increase the sensitivity of CLI, Kothapalli et al. proposed the transmittal of Cerenkov light through different clinical endoscopes and conventional optical fibers. They constructed an optical endoscopy imaging system, shown in Figure 6(a), in which a CCD camera was uncoupled with a 6 mm fiber-optic bundle, shown in Figure 6(b), and used their system to successfully detect as low as 1 μCi of radioactivity emitted from ^{18}F-FDG, as shown in Figure 6(c) [96]. With the development of endoscopic CI, Liu et al. built an optical endoscopy imaging system [97], shown in Figure 7, using a CCD

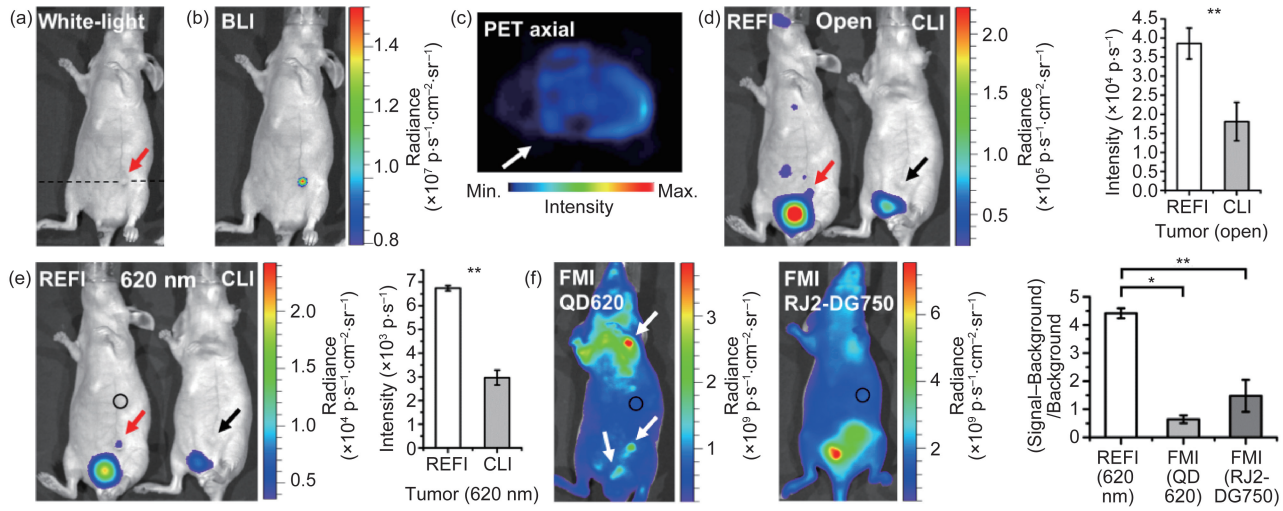

Figure 5. Multimodality comparison for the *in vivo* early detection of small tumor lesions. (a) Sixty-five hours after tumor-cell injection, a photograph shows a small tumor lesion (red arrow). (b) BLI confirms the location of the small tumor lesion. (c) Axial PET shows a false-negative scan. Both (d) without filtering and (e) with 620 nm filtering, CLI (right mouse in each image) shows a false-negative detection (black arrows), but REFI (left mouse) shows true positive detection (red arrows). (f) Fluorescence molecular imaging (FMI) of untargeted QD620 shows multiple suspected lesions, and targeted RJ2-DG750 shows overestimation of the tumor region. The signal-to-background ratios of both fluorescent probes are significantly lower than that of REFI. Reproduced from Ref. [80].

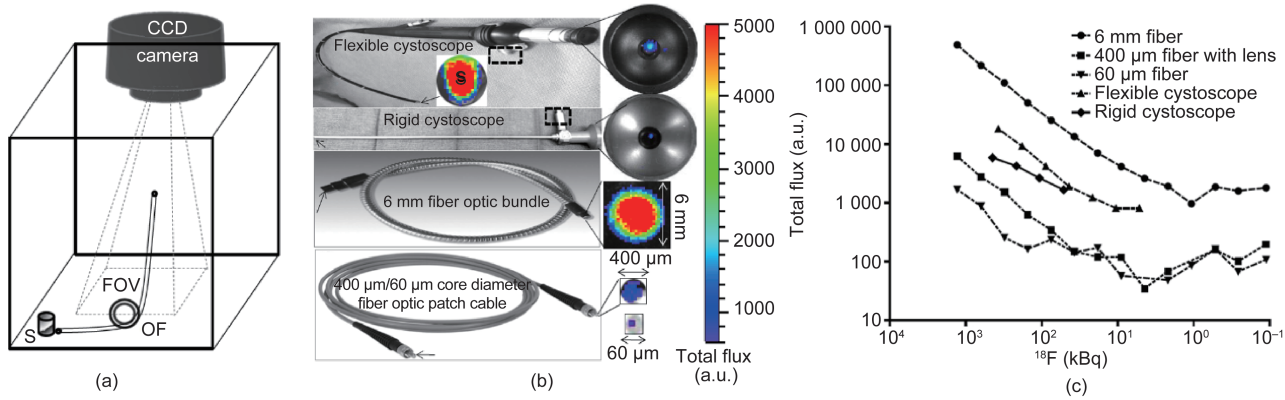

Figure 6. (a) An IVIS-200 spectrum imaging system was adapted to image phantom samples/animal subjects (denoted by "S") pre-administered with ^{18}F-FDG, using different optical fibers (OF) and endoscopes. The subject "S" is placed outside the rectangular field-of-view (FOV) of the imaging system. The input end of the OF is placed close to the subject "S". The output end of the OF faces the CCD camera, which is focused on the output end. (b) A phantom sample (0.2 mL PCR tube) containing about 10 μCi of ^{18}F-FDG in 10 μL of phosphate-buffered saline (PBS) was imaged using different OFs and endoscopes with a 1 min exposure time. Arrows in all figures indicate the distal end of the respective instruments that are within 1 mm of the phantom sample. (c) Detection limits of various optical endoscopes and fibers. Luminescence detected by different fibers as a function of concentration of ^{18}F-FDG with 1 min exposure time. Reproduced from Ref. [96].

camera (Turbo 640-Z; Stanford Photonics Inc., Palo Alto, CA, USA) coupled with an optical imaging fiber bundle that was 108 mm long, shown in Figure 7(a). The distal end of the fiber, shown in Figure 7(b), was coupled with a micro-imaging lens (Cinegon, F/1.4, 12-mm focal length; Schneider, Rueil Malmaison, France).

Intraoperative surgical guiding systems based on CLI have been demonstrated by Holland et al. [98] and Thorek et al. [99]. Holland et al. targeted HER2/neu-positive expressed BT-474 subcutaneous tumors with ^{89}Zr-DFO-trastuzumab and performed a dissection of the BT-474 tumor under the guidance of CLI. Thorek et al. demonstrated the utilization of CLI to aid in the resection of sentinel lymph nodes [99]. Liu et al. [97] demonstrated the feasibility of utilizing a Cerenkov luminescence endoscopy (CLE) system to guide the resection of tumor tissues with an *in vivo* tumor imaging study, depicted in Figure 7(c) and (d). With further improvements in sensitivity and spatial resolution, clinical applications of CLE systems may arise in the near future.

CLI and CLE acquire only superficial scattered and attenuated CL; therefore, they lose more accuracy as the depth of the radiotracer source increases. In 2010, two groups of researchers developed Cerenkov luminescence tomography (CLT) systems independently. Li et al. [100] measured the Cerenkov optical luminescence with a commercial optical imaging system (Caliper IVIS 100) and acquired a micro-PET scan (micro-PET II scanner) for the validation of radiotracer distribution and a micro-CT scan (Inveon, Siemens Preclinical Solutions) for anatomic reference. As shown in Figure 8, due to the placement of two side mirrors, the CCD camera simultaneously captured images of the emitted photons from the top and from two side surfaces. Hu et al. used a dual-modality ZKKS-Direct3D molecular imaging system, including a scientific liquid-cooled back-illuminated CCD camera (Princeton Instruments PIXIS 2048B, Roper Scientific, Trenton, NJ, USA) and a micro-CT system consisting of a micro-focus X-ray source (Oxford Instruments Series5000 Apogee, CA, USA), to localize the implanted radioactive sources by

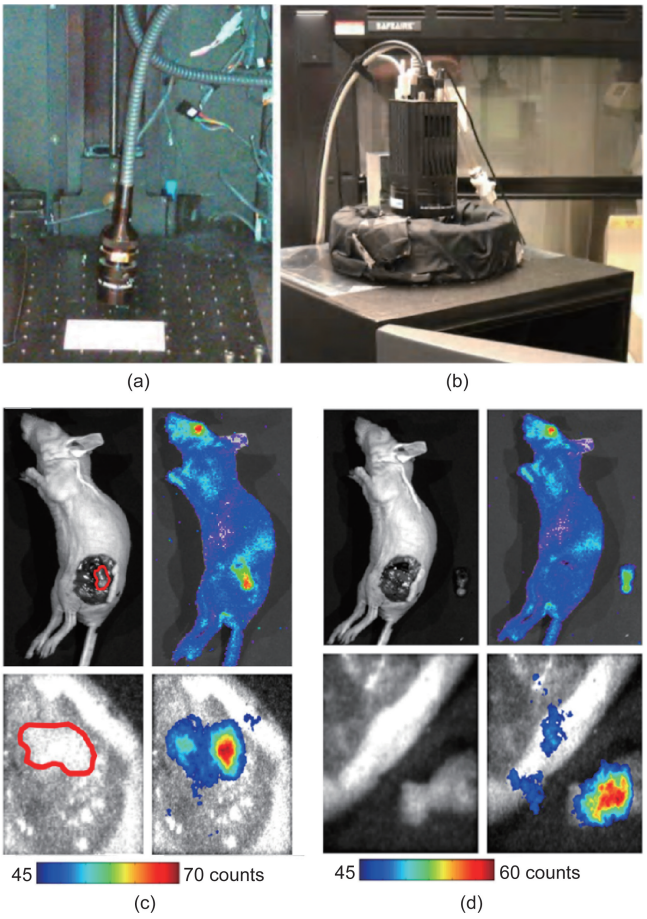

Figure 7. A prototype of a fiber-based system for endoscopic and laparoscopic CLI applications. (a) An optical fiber with a micro-imaging lens was coupled to (b) an image-intensified CCD. (c) Mouse 1, bearing C6 glioma after tail-vein administration of 37 MBq (1 mCi) of ^{18}F-FDG. The mouse was imaged by a commercially available optical IVIS system and by a fiber-based system; tumor tissues are outlined by red lines. Ambient-light images are on the left and fused images are on the right. (d) Mouse 1 was imaged by an IVIS optical system and by a fiber-based system after surgery to remove tumor tissues. Ambient-light images are on the left and fused images are on the right. Reproduced from Ref. [97].

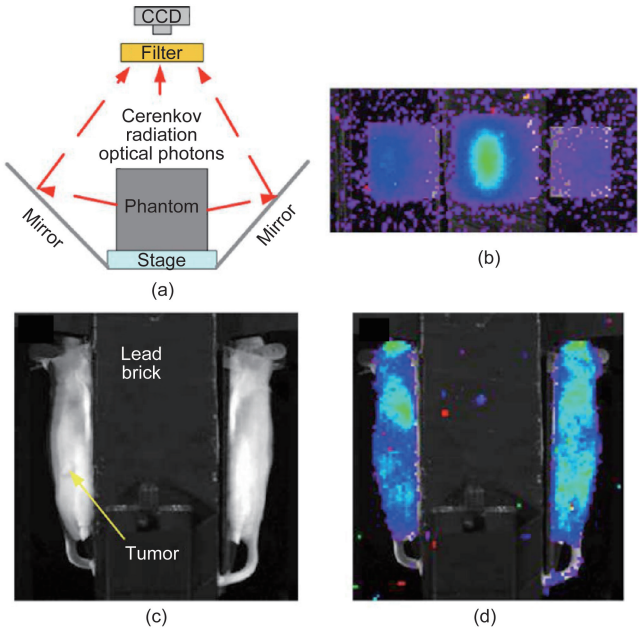

Figure 8. (a) Schematic diagram of the Cerenkov optical acquisition setup of the system by Li et al. (b) CL measurement from phantom. (c) Experimental setup for *in vivo* measurement. (d) CL measurements from two side views. Reproduced from Ref. [100].

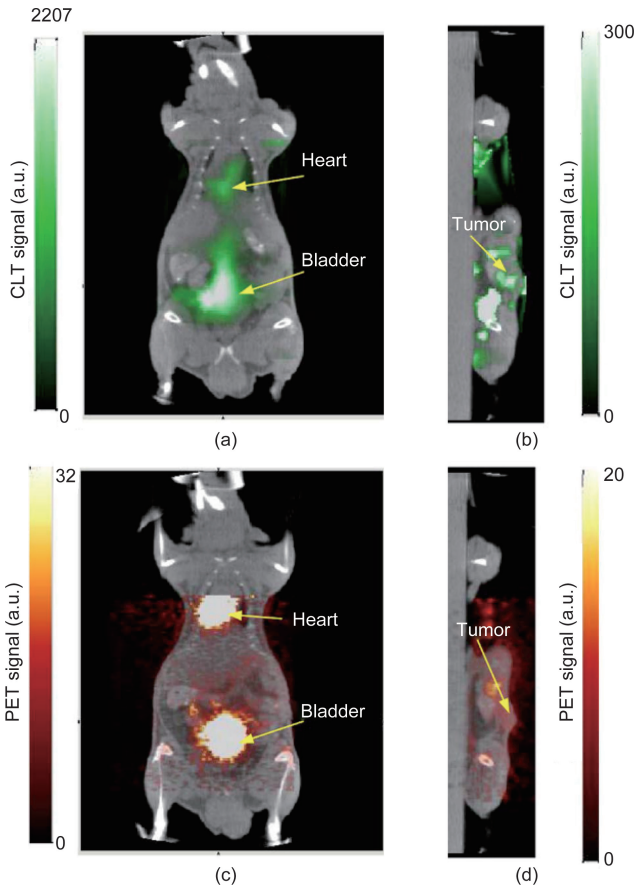

Figure 9. Reconstructed CLT images fused with micro-CT images. (a) Coronal cross-section showing the bladder and heart and (b) sagittal cross-section at tumor. (c) & (d) Corresponding fused micro-PET/CT images. Reproduced from Ref. [100].

3D reconstruction; they achieved distance errors in the low millimeter range, compared with CLT and SPECT [101]. The anesthetized mouse was affixed to the animal-imaging holder and placed on the rotation stage.

The early CLT reconstruction method adopted the radiative transfer equation (RTE) to describe the photon transport problem. The mouse was assumed to be homogeneous and all the optical parameters were set by the same value over the whole body [100] (Figure 9). Hu et al. introduced the CT data as the prior information in order to establish the heterogeneous model [101]. As shown in Figure 10, the heterogeneous model fuses the CT data and optical data successfully and improves the reconstruction accuracy. Spinelli et al. introduced multispectral information to reconstruct the radiotracers; this method not only improves the reconstruction accuracy but also simplifies the detecting devices [102]. All of the methods mentioned above adopt the diffusion equation in order to approximate the RTE. The diffusion equation loses its accuracy in spectrums with short wavelengths, such as the blue spectrum. As most emitting photons in Cerenkov radiance are in the blue-light spectrum, and the light intensity is inversely proportional to the square of the wavelength, the diffusion equation is not very appropriate for CLT reconstruc-

tion. Therefore, a third-order simplified spherical harmonics approximation of RTE was employed to model Cerenkov photon propagation by Zhong et al. [103] (Figure 11). More studies were done to reduce the reconstruction time [104].

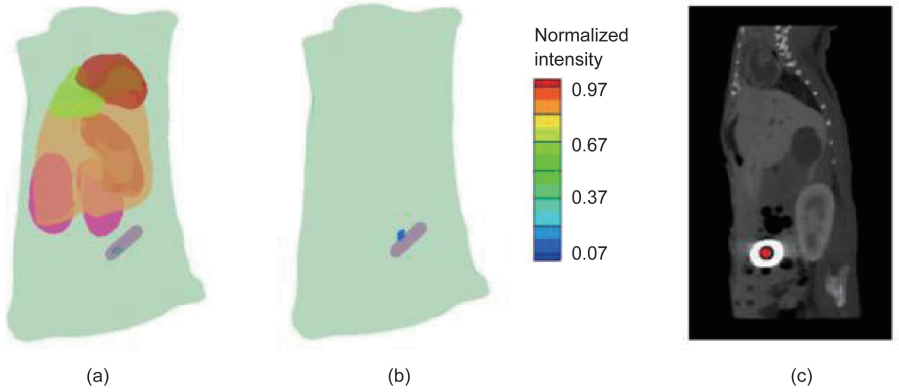

Figure 10. CLT reconstruction of the radioactive source distribution in a mouse with an implanted 600 μCi $Na^{131}I$ radioactive source. (a) & (b) The 3D renderings of the reconstructed source distribution in (a) heterogeneous and (b) homogeneous mouse models. (c) The true source (inside the black circle) in a micro-CT slice superimposed with the reconstructed source (red triangle) from a sagittal view. Reproduced from Ref. [101].

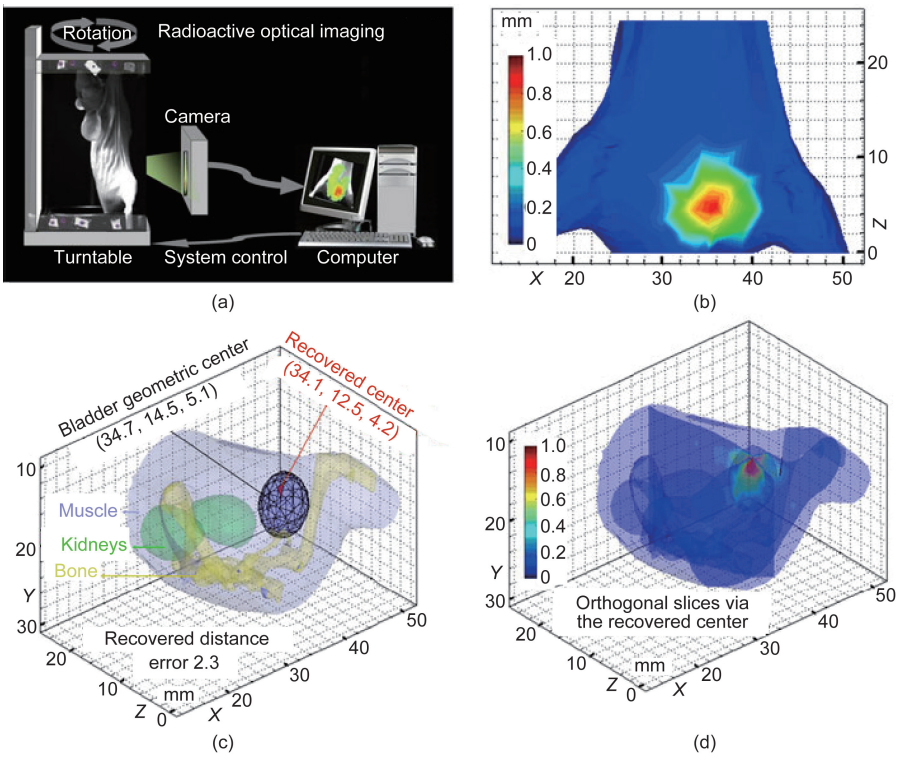

Figure 11. *In vivo* application of whole-body CLT via finite element SP3 approximation with ^{18}F-FDG. (a) Schematic diagram of the system setup in radioactive optical imaging. (b) Planar optical signal distribution on the body surface, which was around the bladder area with high radiotracer accumulation. (c) The mouse was discredited into the tetrahedral mesh as the input of the SP3 model, including 3555 nodes, 38 115 triangles, and 18 690 tetrahedrons. The reconstructed light source center was inside the bladder with the maximum light intensity of 4.4×10^{-12} W·mm^{-3}. (d) Orthogonal slices via the recovered center demonstrated the distribution of radiotracer inside the bladder three-dimensionally. Reproduced from Ref. [103].

4 Intraoperative surgical navigation systems using OMI

Current medical imaging techniques play an important role in the field of preoperative diagnosis and post-operative evaluations. However, with regards to intraoperative imaging technology, the most frequently used imaging modalities were surgeons' eyes and hands. Novel techniques that can extent a surgeon's vision and sense of touch are desired. Existing medical imaging techniques such as CT, MRI, and PET can image a tumor that is larger than 5 mm in human applications [105]. However, more sensitive and accurate imaging technologies are urgently required. The rising technology of OMI shows great superiority in clinical translations. Fluorescence molecular imaging (FMI) technology, a branch of OMI, has been applied to several clinical surgeries such as ovarian cancer [106], early stage esophageal cancer diagnosis [107], and sentinel lymph node (SLN) detection [108]. There are three principal advantages in using FMI for complex intraoperative applications: ① high sensitivity and specificity in the detection of micro lesions; ② real-time imaging at the detection area during the dissection process; and ③ no radiation or contact with tissues, resulting in no influence on traditional surgery procedures. Current studies have already proved the high sensitivity and accuracy of micro-tumor dissection using FMI systems in clinical applications.

To achieve superior sensitivity and accuracy in clinical translations and to fulfill clinical demands, novel medical instruments should include three important features in addition to obtaining FDA certification: ① multispectral visualization including white light and lesion-specific fluorescence; ② optimized fluorescence detection and sufficient light sources for excitation; ③ convenient manipulation for surgeons. Among all other imaging challenges, detection depth is the major issue for the FMI technique. In order to achieve a high signal-to-background ratio (SBR) during surgery, the first NIR window is commonly used, in which light absorption and scattering are relatively low and cannot be seen by the naked eye [109]. Many academic and commercial systems based on the principle of fluorescence imaging are available for clinical applications [110–123]. Milestone studies, such as precise cancer imaging and nerve-damage protection surgery, have been performed that aimed for increasing the precision in intraoperative applications [124, 125].

Several academic and commercial

intraoperative FMI systems are currently available for clinical applications (Figure 12). Depending on the surgical application, these systems can be classified as either open-surgery or endoscopic FMI systems. Furthermore, different types of FMI systems have different advantages due to a focus on different features.

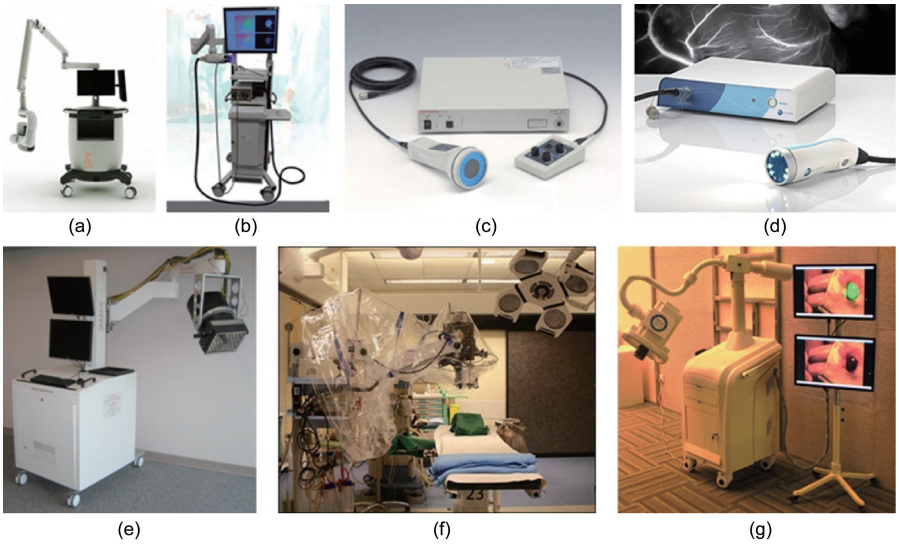

Figure 12. Intraoperative FMI systems. (a) The Novadaq SPY™ system. (b) Artemis™. (c) Hamamatsu's Photodynamic Eye (PDE™). (d) Fluoptics' Fluobeam®, Functional intraoperative FMI systems. (e) FLARE™ imaging system. (f) Multispectral FMI system from Technische Universität München & Helmholtz Zentrum. (g) Surgical navigation system GXMI Navigator from the Institute of Automation, Chinese Academy of Sciences [126].

4.1 Intraoperative FMI systems for open surgery

Multispectral intraoperative FMI systems have advantages in image acquiring and processing. The FLARE™ system was developed by the Frangioni Laboratory, Department of Radiology, Beth Israel Deaconess Medical Center (www.frangionilab.org), Harvard Medical School. This system uses dual NIR channels and a white-light channel to simultaneously collect images. Three CCD cameras are used to collect images in different spectrums: The NIR channel 1 is used to collect light above 800 nm, the NIR channel 2 is used to collect light between 700–800 nm, and the white-light camera is used to collect light between 400–650 nm. The excitation light usually used involves two components: halogen for white light at 40 000 lux and LEDs for NIR light (4 mW·cm^{-2} of 670 nm and 11 mW·cm^{-2} of 760 nm). For the image results, different NIR images are pseudocolored with red and green, respectively, and merged onto the white-light images. In terms of real-time imaging, the FLARE and mini FLARE systems acquire and display images at a rate of 15 fps. This academic system has been used in several clinical applications such as cancer surgery and SLN mapping [115, 127–130].

Another multispectral FMI system was developed by Technische Universität München and Helmholtz Zentrum (http://www.helmholtz-muenchen.de), and is similar to the FLARE system. This system has the advantage of imaging processing that corrects for attenuation from the excitation light, and has been remarkably applied to human ovarian cancer surgery [106, 131–134]. Another FMI system was developed in the Key Laboratory of Molecular Imaging, Chinese Academy of Sciences (http://www.3dmed.net/), and has the advantage of convenient operation. This system also improves the quality of image results by using feature point algorithms in order to ensure rapid and precise imaging fusion for the two cameras in the system [135]. The system has been successfully applied in breast cancer SLN mapping and liver cancer detection in clinics.

As intraoperative FMI systems aim to assist surgeons in precision surgery, convenient designs were considered in many commercial products. The first FDA-approved FMI product was the SPY™ system developed by Novadaq Technologies, Inc. (www.novadaq.com). It showed previous application in the field of vessel bypass surgery. Recently, the SPY™ system has been applied to accurately identify mastectomy-flap necrosis with the fluorescence imaging agent indocyanine green (ICG) in 62 breast-reconstruction cases during surgery [136]. The Photodynamic Eye (PDE™), produced by Hamamatsu Photonics, is approved by the FDA for clinical applications including SLN detection in breast cancer [137, 138] and liver cancer surgery [139]. This handheld imaging system emits annular 760 nm LED NIR light and uses a single CCD camera to detect the reflected fluorescence light. As LED light energy is limited, the image quality has great potential for improvement for further operation-room applications. Another handheld product designed by Fluoptics (www.fluoptics.com), named Fluobeam®, has similar functions as the PDE™ and has been used in clinical trials aiming to prove its feasibility during surgery. In addition, Artemis™ simultaneously shows the color image and the fluorescent overlay, which provides excellent utility for nerve surgery [140, 141]. Nerve preservation is an important issue during most surgery because accidental transection or injury results in significant morbidity. NIR window I fluorescent light has the potential to provide high resolution, high sensitivity, and real-time avoidance of nerve damage. By using a fluorescent probe, FMI imaging can image the nerves in human tissue samples. Fluorescence highlighting is independent of axonal integrity, suggesting that the probe could facilitate the surgical repair of injured nerves and help prevent accidental transection [142, 143].

4.2 Intraoperative FMI systems for endoscopic surgery

Recently, novel fluorescence endoscopic and laparoscopic systems were designed to realize minimal invasiveness and to solve the detection-depth problem during surgery [144]. The most commercial endoscope systems use 400–700 nm visible-light-spectrum fluorescence imaging, which is similar to an ordinary white-light image. However, the lack of contrast between lesions and normal tissue makes it difficult for surgeons to decide where to

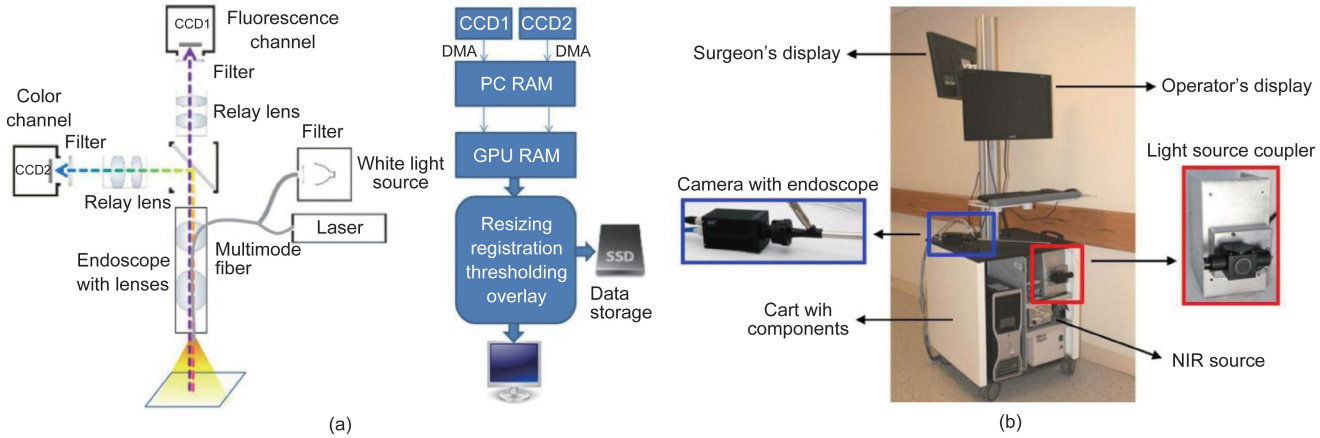

Figure 13. Design of endoscopic FMI system. (a) Schematic of the intraoperative imaging system and software pipeline [145]; (b) the clinically applied dual-channel endoscopic imaging system [146].

dissect. In order to detect early micro-tumor lesions and improve the effects of treatment, several endoscopic techniques such as image-enhanced endoscopy, endoscopic microscopy, and NIR fluorescence endoscopy were used to improve diagnosis accuracy. Because the NIR FMI technique showed great superiority in intraoperative high-SBR imaging, some novel NIR endoscopic FMI systems were designed for intraoperative image-guided surgery (Figure 13).

The challenging problem of how to design the endoscopic optical path to simultaneously achieve white-light and NIR fluorescent images has limited most fluorescence endoscopic imaging systems. An NIR fluorescence endoscopic system should balance the sensitivity and size of the image detector, the optical coupling efficiency, and the excitation energy. Glatz et al. used an electron multiplying charge-coupled device (EMCCD) to increase the detection sensitivity of significant contrast between tumors and normal tissues and evaluated their system for the identification of colorectal tumor margins [145]. Venugopal et al. reported a unique optical path design to simultaneously achieve color and NIR fluorescence images [146]. This prism-based 2-CCD camera endoscopic imaging system, which is compatible with two light sources in color and in the NIR range, realized one hand operation and real-time imaging registration during surgery. Furthermore, thoracic SLN mapping in a porcine model validated the feasibility of the system performance.

For clinical translations, Hide et al. addressed a recurrent intracavernous sinus dermoid cyst using an NIR endoscopic system in order to confirm the patency of the internal carotid artery and the cavernous sinus. This NIR endoscope was superior for real-time imaging and a high SBR for the lesions, and showed great value for successful endonasal transsphenoidal surgery [147]. Plante et al. reported a pilot study using a novel endoscopic FMI system for SLN mapping in cervical and endometrial cancer with ICG [148]. The results showed that with the help of an NIR FMI system, SLN mapping detection can achieve a very high overall (96%) and bilateral (88%) rate. Pan et al. used fluorescence imaging systems, confocal endomicroscopy, and blue light cystoscopy in fresh surgically removed human bladders with fluorescently labeled CD47 antibody (anti-CD47) as molecular imaging agent for accurate diagnosis and image-guided surgery. The results showed 82.9% sensitivity and 90.5% specificity, which improved diagnosis and resection thoroughness for bladder cancer [149].

In summary, intraoperative surgical navigation systems using FMI technology can extend the vision of surgeons, enabling them to precisely distinguish lesions from normal tissues, and improving surgery sensitivity and accuracy for many important biological applications and clinical translations [150].

5 Perspectives

In the past decade, as more and more researchers and clinicians realize the significance of precise medicine and personalized cancer-patient treatment based on a fundamental understanding of cancer biology at the cellular and molecular level, enormous strides have been made in the field of *in vivo* OMI and its clinical translations. With this strong motivation, many new optical imaging systems, algorithms, agents, and reporters have been applied to cancer research, new therapy development, and clinical patient care.

Optical multimodality imaging has transformed the optical observation of molecular processes and events from a crude qualitative planar approach to a quantitative 3D imaging technique. Small-animal whole-body biodistribution, the targeting specificity and pharmacokinetics of optical molecular probes, and the tumor-cell response to therapeutic interventions can all be imaged accurately and dynamically in intact host environments. Important biological information, such as tumor marker expression, available reporter density, and lymph node tumor burden quantification, which in the past could only be accessed by analyzing select tissue specimens extracted by biopsy or tumor tissue resection, can now be analyzed *in vivo* with unprecedented accuracy and sensitivity.

CLI has provided a new pathway to imaging clinically approved radioactive tracers with optical-based technologies, and exhibits many advantages. This technique has the potential to accelerate the speed of clinical translation for OMI, as the majority of fluorescence probes are still limited in preclinical applications. The combination of nuclear and optical imaging, the two most sensitive imaging modalities,

may break through the current sensitivity limitation of *in vivo* early-tumor imaging and may provide a way to observe tumor progression at a much earlier stage.

The clinical translation of OMI has been slower than was initially hoped for. The reasons behind this slower translation are complex, but one of the biggest problems involves the regulatory hurdles for optical molecular probes. However, imaging systems and strategies have moved forward by exploring the potential clinical applications of FDA-approved optical imaging agents such as ICG. Intraoperative fluorescent image-guided surgery has become well-accepted in clinical trials, with promising tumor-resection accuracy in tumor-margin definition and superb sensitivity in tiny tumor foci or residual detection. The outdated perception of lower market profit margins for OMI than for therapeutic drugs is gradually changing.

With recent advances in OMI technologies, we believe that more and more unverified biomedical hypotheses can be investigated using more powerful imaging strategies, and significant new discoveries in oncology can be achieved through imaging observation. The more accurate and sensitive imaging studies performed using OMI have enabled researchers to obtain a deeper and better understanding of molecular processes and evens of cancer—an understanding that is likely to motivate even faster development of OMI in the next decade. The clinical translation of these novel imaging technologies will continue and accelerate. Applying these new optical imaging technologies to human healthcare will lead to a fundamental improvement in diagnostic and therapeutic cancer interventions. In the era of molecular imaging, optical technologies hold great promise to facilitate the development of highly accurate and sensitive cancer diagnoses as well as personalized patient treatment—one of the ultimate goals of precision medicine.

Compliance with ethics guidelines

Kun Wang, Chongwei Chi, Zhenhua Hu, Muhan Liu, Hui Hui, Wenting Shang, Dong Peng, Shuang Zhang, Jinzuo Ye, Haixiao Liu, and Jie Tian declare that they have no conflict of interest or financial conflicts to disclose.

References

1. J. R. Conway, N. O. Carragher, P. Timpson. Developments in preclinical cancer imaging: Innovating the discovery of therapeutics. *Nat. Rev. Cancer*, 2014, 14(5): 314–328
2. T. Maldiney, et al. The *in vivo* activation of persistent nanophosphors for optical imaging of vascularization, tumours and grafted cells. *Nat. Mater.*, 2014, 13(4): 418–426
3. S. I. Ellenbroek, J. van Rheenen. Imaging hallmarks of cancer in living mice. *Nat. Rev. Cancer*, 2014, 14(6): 406–418
4. R. Weissleder, M. J. Pittet. Imaging in the era of molecular oncology. *Nature*, 2008, 452(7187): 580–589
5. Z. Hu, et al. From PET/CT to PET/MRI: Advances in instrumentation and clinical applications. *Mol. Pharm.*, 2014, 11(11): 3798–3809
6. J. S. Reynolds, et al. Imaging of spontaneous canine mammary tumors using fluorescent contrast agents. *Photochem. Photobiol.*, 1999, 70(1): 87–94
7. U. Mahmood, C. H. Tung, A. Bogdanov Jr., R. Weissleder. Near-infrared optical imaging of protease activity for tumor detection. *Radiology*, 1999, 213(3): 866–870
8. M. Yang, et al. Whole-body optical imaging of green fluorescent protein-expressing tumors and metastases. *Proc. Natl. Acad. Sci. U.S.A.*, 2000, 97(3): 1206–1211
9. V. Ntziachristos, J. Ripoll, L. V. Wang, R. Weissleder. Looking and listening to light: The evolution of whole-body photonic imaging. *Nat. Biotechnol.*, 2005, 23(3): 313–320
10. C. Qin, et al. Recent advances in bioluminescence tomography: Methodology and system as well as application. *Laser Photonics Rev.*, 2014, 8(1): 94–114
11. V. Ntziachristos. Going deeper than microscopy: The optical imaging frontier in biology. *Nat. Methods*, 2010, 7(8): 603–614
12. F. Leuschner, M. Nahrendorf. Molecular imaging of coronary atherosclerosis and myocardial infarction: Considerations for the bench and perspectives for the clinic. *Circ. Res.*, 2011, 108(5): 593–606
13. S. R. Arridge, M. Schweiger, M. Hiraoka, D. T. Delpy. A finite element approach for modeling photon transport in tissue. *Med. Phys.*, 1993, 20(2): 299–309
14. H. L. Graber, R. L. Barbour. High-resolution near-infrared (NIR) imaging of dense scattering media by diffusion tomography. *Faseb J.*, 1993, 7: A720
15. J. C. Schotland, J. S. Leigh. Photon diffusion imaging. *Faseb J.*, 1992, 6: A446–A446
16. A. Yodh, B. Chance. Spectroscopy and imaging with diffusing light. *Phys. Today*, 1995, 48(3): 34–40
17. M. S. Patterson, B. Chance, B. C. Wilson. Time resolved reflectance and transmittance for the non-invasive measurement of tissue optical properties. *Appl. Opt.*, 1989, 28(12): 2331–2336
18. B. Chance. Optical method. *Annu. Rev. Biophys. Biophys. Chem.*, 1991, 20: 1–28
19. F. F. Jöbsis. Noninvasive, infrared monitoring of cerebral and myocardial oxygen sufficiency and circulatory parameters. *Science*, 1977, 198(4323): 1264–1267
20. A. M. Smith, M. C. Mancini, S. Nie. Bioimaging: Second window for *in vivo* imaging. *Nat. Nanotechnol.*, 2009, 4(11): 710–711
21. R. Weissleder. A clearer vision for *in vivo* imaging. *Nat. Biotechnol.*, 2001, 19(4): 316–317
22. D. Zhu, C. Li. Nonconvex regularizations in fluorescence molecular tomography for sparsity enhancement. *Phys. Med. Biol.*, 2014, 59(12): 2901–2912
23. D. Han, et al. A fast reconstruction algorithm for fluorescence molecular tomography with sparsity regularization. *Opt. Express*, 2010, 18(8): 8630–8646
24. K. Liu, et al. Tomographic bioluminescence imaging reconstruction via a dynamically sparse regularized global method in mouse models. *J. Biomed. Opt.*, 2011, 16(4): 046016
25. Y. Lv, et al. A multilevel adaptive finite element algorithm for bioluminescence tomography. *Opt. Express*, 2006, 14(18): 8211–8223
26. J. Zhong, J. Tian, X. Yang, C. Qin. Whole-body Cerenkov luminescence tomography with the finite element SP(3) method. *Ann. Biomed. Eng.*, 2011, 39(6): 1728–1735
27. X. Ding, K. Wang, B. Jie, Y. Luo, Z. Hu, J. Tian. Probability method for Cerenkov luminescence tomography based on conformance error minimization. *Biomed. Opt. Express*, 2014, 5(7): 2091–2112
28. A. Ale, V. Ermolayev, E. Herzog, C. Cohrs, M. H. de Angelis, V. Ntziachristos. FMT-XCT: *In vivo* animal studies with hybrid fluorescence molecular tomography-X-ray computed tomography. *Nat. Methods*, 2012, 9(6):

615–620
29. P. Mohajerani, et al. FMT-PCCT: Hybrid fluorescence molecular tomography-X-ray phase-contrast CT imaging of mouse models. *IEEE Trans. Med. Imaging*, 2014, 33(7): 1434–1446
30. S. C. Davis, et al. Magnetic resonance-coupled fluorescence tomography scanner for molecular imaging of tissue. *Rev. Sci. Instrum.*, 2008, 79(6): 064302
31. M. J. Eppstein, D. J. Hawrysz, A. Godavarty, E. M. Sevick-Muraca. Three-dimensional, Bayesian image reconstruction from sparse and noisy data sets: Near-infrared fluorescence tomography. *Proc. Natl. Acad. Sci. U.S.A.*, 2002, 99(15): 9619–9624
32. X. Gu, Q. Zhang, L. Larcom, H. Jiang. Three-dimensional bioluminescence tomography with model-based reconstruction. *Opt. Express*, 2004, 12(17): 3996–4000
33. C. Li, G. S. Mitchell, S. R. Cherry. Cerenkov luminescence tomography for small-animal imaging. *Opt. Lett.*, 2010, 35(7): 1109–1111
34. K. Liu, et al. Evaluation of the simplified spherical harmonics approximation in bioluminescence tomography through heterogeneous mouse models. *Opt. Express*, 2010, 18(20): 20988–21002
35. H. Liu, et al. Multispectral hybrid Cerenkov luminescence tomography based on the finite element SP_n method. *J. Biomed. Opt.*, 2015, 20(8): 086007
36. D. Zhu, C. Li. Nonuniform update for sparse target recovery in fluorescence molecular tomography accelerated by ordered subsets. *Biomed. Opt. Express*, 2014, 5(12): 4249–4259
37. D. Wang, X. Song, J. Bai. Adaptive-mesh-based algorithm for fluorescence molecular tomography using an analytical solution. *Opt. Express*, 2007, 15(15): 9722–9730
38. N. Cao, A. Nehorai, M. Jacobs. Image reconstruction for diffuse optical tomography using sparsity regularization and expectation-maximization algorithm. *Opt. Express*, 2007, 15(21): 13695–13708
39. J. Dutta, S. Ahn, C. Li, S. R. Cherry, R. M. Leahy. Joint L1 and total variation regularization for fluorescence molecular tomography. *Phys. Med. Biol.*, 2012, 57(6): 1459–1476
40. D. Han, et al. Sparsity-promoting tomographic fluorescence imaging with simplified spherical harmonics approximation. *IEEE Trans. Biomed. Eng.*, 2010, 57(10): 2564–2567
41. J. Shi, F. Liu, G. Zhang, J. Luo, J. Bai. Enhanced spatial resolution in fluorescence molecular tomography using restarted L1-regularized nonlinear conjugate gradient algorithm. *J. Biomed. Opt.*, 2014, 19(4): 046018
42. P. Wu, et al. Detection of mouse liver cancer via a parallel iterative shrinkage method in hybrid optical/microcomputed tomography imaging. *J. Biomed. Opt.*, 2012, 17(12): 126012
43. P. Wu, Y. Hu, K. Wang, J. Tian. Bioluminescence tomography by an iterative reweighted (l)2 norm optimization. *IEEE Trans. Biomed. Eng.*, 2014, 61(1): 189–196
44. S. C. Davis, et al. Dynamic dual-tracer MRI-guided fluorescence tomography to quantify receptor density *in vivo*. *Proc. Natl. Acad. Sci. U.S.A.*, 2013, 110(22): 9025–9030
45. X. Ma, et al. SM5-1-conjugated PLA nanoparticles loaded with 5-fluorouracil for targeted hepatocellular carcinoma imaging and therapy. *Biomaterials*, 2014, 35(9): 2878–2889
46. Y. Liu, S. J. Redmond, N. Wang, F. Blumenkron, M. R. Narayanan, N. H. Lovell. Spectral analysis of accelerometry signals from a directed-routine for falls-risk estimation. *IEEE Trans. Biomed. Eng.*, 2011, 58(8): 2308–2315
47. X. Liu, B. Zhang, J. Luo, J. Bai. 4-D reconstruction for dynamic fluorescence diffuse optical tomography. *IEEE Trans. Med. Imaging*, 2012, 31(11): 2120–2132
48. F. Leuschner, et al. Therapeutic siRNA silencing in inflammatory monocytes in mice. *Nat. Biotechnol.*, 2011, 29(11): 1005–1010
49. Y. Lin, D. Thayer, O. Nalcioglu, G. Gulsen. Tumor characterization in small animals using magnetic resonance-guided dynamic contrast enhanced diffuse optical tomography. *J. Biomed. Opt.*, 2011, 16(10): 106015
50. K. M. Tichauer, et al. Microscopic lymph node tumor burden quantified by macroscopic dual-tracer molecular imaging. *Nat. Med.*, 2014, 20(11): 1348–1353
51. Q. Zhang, Y. Du, Z. Xue, C. Chi, X. Jia, J. Tian. Comprehensive evaluation of the anti-angiogenic and anti-neoplastic effects of Endostar on liver cancer through optical molecular imaging. *PLoS ONE*, 2014, 9(1): e85559
52. C. H. Contag, M. H. Bachmann. Advances in *in vivo* bioluminescence imaging of gene expression. *Annu. Rev. Biomed. Eng.*, 2002, 4: 235–260
53. M. Keyaerts, V. Caveliers, T. Lahoutte. Bioluminescence imaging: Looking beyond the light. *Trends Mol. Med.*, 2012, 18(3): 164–172
54. K. Hochgräfe, E. M. Mandelkow. Making the brain glow: *In vivo* bioluminescence imaging to study neurodegeneration. *Mol. Neurobiol.*, 2013, 47(3): 868–882
55. M. F. Kircher, et al. A brain tumor molecular imaging strategy using a new triple-modality MRI-photoacoustic-Raman nanoparticle. *Nat. Med.*, 2012, 18(5): 829–834
56. A. G. Bell. On the production and reproduction of sound by light. *Am. J. Sci.*, 1880, s3-20(118): 305–324
57. S. Zackrisson, S. M. van de Ven, S. S. Gambhir. Light in and sound out: Emerging translational strategies for photoacoustic imaging. *Cancer Res.*, 2014, 74(4): 979–1004
58. L. V. Wang, L. Gao. Photoacoustic microscopy and computed tomography: From bench to bedside. *Annu. Rev. Biomed. Eng.*, 2014, 16: 155–185
69. L. V. Wang, S. Hu. Photoacoustic tomography: *In vivo* imaging from organelles to organs. *Science*, 2012, 335(6075): 1458–1462
60. A. Taruttis, V. Ntziachristos. Advances in real-time multispectral optoacoustic imaging and its applications. *Nat. Photonics*, 2015, 9(4): 219–227
61. G. Hong, et al. Multifunctional *in vivo* vascular imaging using near-infrared II fluorescence. *Nat. Med.*, 2012, 18(12): 1841–1846
62. G. Hong, et al. Ultrafast fluorescence imaging *in vivo* with conjugated polymer fluorophores in the second near-infrared window. *Nat. Commun.*, 2014, 5: 4206
63. G. Hong, et al. Through-skull fluorescence imaging of the brain in a new near-infrared window. *Nat. Photonics*, 2014, 8(9): 723–730
64. R. K. O'Reilly, C. J. Hawker, K. L. Wooley. Cross-linked block copolymer micelles: Functional nanostructures of great potential and versatility. *Chem. Soc. Rev.*, 2006, 35(11): 1068–1083
65. L. M. Ensign, et al. Mucus-penetrating nanoparticles for vaginal drug delivery protect against herpes simplex virus. *Sci. Transl. Med.*, 2012, 4(138): 138ra79
66. J. Ezzati Nazhad Dolatabadi, H. Valizadeh, H. Hamishehkar. Solid lipid nanoparticles as efficient drug and gene delivery systems: Recent breakthroughs. *Adv. Pharm. Bull.*, 2015, 5(2): 151–159
67. X. Q. Zhang, X. Xu, R. Lam, D. Giljohann, D. Ho, C. A. Mirkin. Strategy for increasing drug solubility and efficacy through covalent attachment to polyvalent DNA-nanoparticle conjugates. *ACS Nano*, 2011, 5(9): 6962–6970
68. K. M. Gharpure, S. Y. Wu, C. Li, G. Lopez-Berestein, A. K. Sood. Nanotechnology: Future of oncotherapy. *Clin. Cancer Res.*, 2015, 21(14): 3121–3130
69. D. Geißler, L. J. Charbonnière, R. F. Ziessel, N. G. Butlin, H. G. Löhmannsröben, N. Hildebrandt. Quantum dot biosensors for ultrasensitive multiplexed diagnostics. *Angew. Chem. Int. Ed. Engl.*, 2010, 49(8): 1396–1401
70. H. Meng, et al. Use of size and a copolymer design feature to improve the biodistribution and the enhanced permeability and retention effect of doxorubicin-loaded mesoporous silica nanoparticles in a murine xenograft tumor model. *ACS Nano*, 2011, 5(5): 4131–4144

71. H. Meng, et al. Codelivery of an optimal drug/siRNA combination using mesoporous silica nanoparticles to overcome drug resistance in breast cancer *in vitro* and *in vivo*. *ACS Nano*, 2013, 7(2): 994–1005
72. R. Qiao, et al. Ultrasensitive *in vivo* detection of primary gastric tumor and lymphatic metastasis using upconversion nanoparticles. *ACS Nano*, 2015, 9(2): 2120–2129
73. K. Ajima, et al. Enhancement of *in vivo* anticancer effects of cisplatin by incorporation inside single-wall carbon nanohorns. *ACS Nano*, 2008, 2(10): 2057–2064
74. V. N. Mochalin, O. Shenderova, D. Ho, Y. Gogotsi. The properties and applications of nanodiamonds. *Nat. Nanotechnol*., 2012, 7(1): 11–23
75. D. L. J. Thorek, A. Ogirala, B. J. Beattie, J. Grimm. Quantitative imaging of disease signatures through radioactive decay signal conversion. *Nat. Med*., 2013, 19(10): 1345–1350
76. H. Liu, et al. Molecular optical imaging with radioactive probes. *PLoS ONE*, 2010, 5(3): e9470
77. A. Ruggiero, J. P. Holland, J. S. Lewis, J. Grimm. Cerenkov luminescence imaging of medical isotopes. *J. Nucl. Med*., 2010, 51(7): 1123–1130
78. A. E. Spinelli, et al. First human Cerenkography. *J. Biomed. Opt*., 2013, 18(2): 020502
79. D. L. J. Thorek, C. C. Riedl, J. Grimm. Clinical Cerenkov luminescence imaging of ^{18}F-FDG. *J. Nucl. Med*., 2014, 55(1): 95–98
80. Z. Hu, et al. *In vivo* nanoparticle-mediated radiopharmaceutical-excited fluorescence molecular imaging. *Nat. Commun*., 2015, 6: 7560
81. R. S. Dothager, R. J. Goiffon, E. Jackson, S. Harpstrite, D. Piwnica-Worms. Cerenkov radiation energy transfer (CRET) imaging: A novel method for optical imaging of PET isotopes in biological systems. *PLoS ONE*, 2010, 5(10): e13300
82. H. Liu, X. Zhang, B. Xing, P. Han, S. S. Gambhir, Z. Cheng. Radiation-luminescence-excited quantum dots for *in vivo* multiplexed optical imaging. *Small*, 2010, 6(10): 1087–1091
83. Y. Bernhard, B. Collin, R. A. Decréau. Inter/intramolecular Cherenkov radiation energy transfer (CRET) from a fluorophore with a built-in radionuclide. *Chem. Commun. (Camb.)*, 2014, 50(51): 6711–6713
84. H. Hu, et al. PET and NIR optical imaging using self-illuminating ^{64}Cu-doped chelator-free gold nanoclusters. *Biomaterials*, 2014, 35(37): 9868–9876
85. X. Sun, et al. Self-illuminating 64Cu-doped CdSe/ZnS nanocrystals for *in vivo* tumor imaging. *J. Am. Chem. Soc*., 2014, 136(5): 1706–1709
86. W. Guo, et al. Intrinsically radioactive [^{64}Cu]CuInS/ZnS quantum dots for PET and optical imaging: Improved radiochemical stability and controllable Cerenkov luminescence. *ACS Nano*, 2015, 9(1): 488–495
87. X. Cao, et al. Intensity enhanced Cerenkov luminescence imaging using terbium-doped Gd_2O_2S microparticles. *ACS Appl. Mater. Interfaces*, 2015, 7(22): 11775–11782
88. I. Veronese, et al. Infrared luminescence for real time ionizing radiation detection. *Appl. Phys. Lett*., 2014, 105(6): 061103
89. Y. Wang, et al. Radioluminescent gold nanocages with controlled radioactivity for real-time *in vivo* imaging. *Nano Lett*., 2013, 13(2): 581–585
90. C. M. Carpenter, C. Sun, G. Pratx, H. Liu, Z. Cheng, L. Xing. Radioluminescent nanophosphors enable multiplexed small-animal imaging. *Opt. Express*, 2012, 20(11): 11598–11604
91. C. Sun, et al. Synthesis and radioluminescence of PEGylated Eu^{3+}-doped nanophosphors as bioimaging probes. *Adv. Mater*., 2011, 23(24): H195–H199
92. O. Volotskova, et al. Efficient radioisotope energy transfer by gold nanoclusters for molecular imaging. *Small*, 2015, 11(32): 4002–4008
93. J. Li, L. W. Dobrucki, M. Marjanovic, E. J. Chaney, K. S. Suslick, S. A. Boppart. Enhancement and wavelength-shifted emission of Cerenkov luminescence using multifunctional microspheres. *Phys. Med. Biol*., 2015, 60(2): 727–739
94. X. Ma, et al. Enhancement of Cerenkov luminescence imaging by dual excitation of Er^{3+},Yb^{3+}-doped rare-earth microparticles. *PLoS ONE*, 2013, 8(10): e77926
95. R. Robertson, M. S. Germanos, C. Li, G. S. Mitchell, S. R. Cherry, M. D. Silva. Optical imaging of Cerenkov light generation from positron-emitting radiotracers. *Phys. Med. Biol*., 2009, 54(16): N355–N365
96. S. R. Kothapalli, H. Liu, J. C. Liao, Z. Cheng, S. S. Gambhir. Endoscopic imaging of Cerenkov luminescence. *Biomed. Opt. Express*, 2012, 3(6): 1215–1225
97. H. Liu, et al. Intraoperative imaging of tumors using Cerenkov luminescence endoscopy: A feasibility experimental study. *J. Nucl. Med*., 2012, 53(10): 1579–1584
98. J. P. Holland, G. Normand, A. Ruggiero, J. S. Lewis, J. Grimm. Intraoperative imaging of positron emission tomographic radiotracers using Cerenkov luminescence emissions. *Mol. Imaging*, 2011, 10(3): 177–186
99. D. L. J. Thorek, et al. Positron lymphography: Multimodal, high-resolution, dynamic mapping and resection of lymph nodes after intradermal injection of 18F-FDG. *J. Nucl. Med*., 2012, 53(9): 1438–1445
100. C. Li, G. S. Mitchell, S. R. Cherry. Cerenkov luminescence tomography for small-animal imaging. *Opt. Lett*., 2010, 35(7): 1109–1111
101. Z. Hu, et al. Experimental Cerenkov luminescence tomography of the mouse model with SPECT imaging validation. *Opt. Express*, 2010, 18(24): 24441–24450
102. A. E. Spinelli, et al. Multispectral Cerenkov luminescence tomography for small animal optical imaging. *Opt. Express*, 2011, 19(13): 12605–12618
103. J. Zhong, J. Tian, X. Yang, C. Qin. Whole-body Cerenkov luminescence tomography with the finite element SP_3 method. *Ann. Biomed. Eng*., 2011, 39(6): 1728–1735
104. J. Zhong, C. Qin, X. Yang, Z. Chen, X. Yang, J. Tian. Fast-specific tomography imaging via Cerenkov emission. *Mol. Imaging Biol*., 2012, 14(3): 286–292
105. B. J. Hillman, J. C. Goldsmith. The uncritical use of high-tech medical imaging. *N. Engl. J. Med*., 2010, 363(1): 4–6
106. G. M. van Dam, et al. Intraoperative tumor-specific fluorescence imaging in ovarian cancer by folate receptor-α targeting: First in-human results. *Nat. Med*., 2011, 17(10): 1315–1319
107. M. B. Sturm, et al. Targeted imaging of esophageal neoplasia with a fluorescently labeled peptide: First-in-human results. *Sci. Transl. Med*., 2013, 5(184): 184ra61
108. S. L. Troyan, et al. The FLARE intraoperative near-infrared fluorescence imaging system: A first-in-human clinical trial in breast cancer sentinel lymph node mapping. *Ann. Surg. Oncol*., 2009, 16(10): 2943–2952
109. B. Chance. Near-infrared images using continuous, phase-modulated, and pulsed light with quantitation of blood and blood oxygenation. *Ann. N.Y. Acad. Sci*., 1998, 838: 29–45
110. B. T. Phillips, et al. Intraoperative perfusion techniques can accurately predict mastectomy skin flap necrosis in breast reconstruction: Results of a prospective trial. *Plast. Reconstr. Surg*., 2012, 129(5): 778e–788e
111. C. Hirche, et al. An experimental study to evaluate the Fluobeam 800 imaging system for fluorescence-guided lymphatic imaging and sentinel node biopsy. *Surg. Innov*., 2013, 20(5): 516–523
112. K. Yamauchi, H. Nagafuji, T. Nakamura, T. Sato, N. Kohno. Feasibility of ICG fluorescence-guided sentinel node biopsy in animal models using the HyperEye Medical System. *Ann. Surg. Oncol*., 2011, 18(7): 2042–2047
113. G. Themelis, J. S. Yoo, K. S. Soh, R. Schulz, V. Ntziachristos. Real-time intraoperative fluorescence imaging system using light-absorption correction. *J. Biomed. Opt*., 2009, 14(6): 064012
114. H. G. van der Poel, T. Buckle, O. R. Brouwer, R. A. Valdés Olmos, F. W.

van Leeuwen. Intraoperative laparoscopic fluorescence guidance to the sentinel lymph node in prostate cancer patients: Clinical proof of concept of an integrated functional imaging approach using a multimodal tracer. *Eur. Urol.*, 2011, 60(4): 826–833

115. S. L. Troyan, et al. The FLARE intraoperative near-infrared fluorescence imaging system: A first-in-human clinical trial in breast cancer sentinel lymph node mapping. *Ann. Surg. Oncol.*, 2009, 16(10): 2943–2952
116. S. Yamashita, et al. Video-assisted thoracoscopic indocyanine green fluorescence imaging system shows sentinel lymph nodes in non-small-cell lung cancer. *J. Thorac. Cardiovasc. Surg.*, 2011, 141(1): 141–144
117. G. Spinoglio, et al. Real-time near-infrared (NIR) fluorescent cholangiography in single-site robotic cholecystectomy (SSRC): A single-institutional prospective study. *Surg. Endosc.*, 2013, 27(6): 2156–2162
118. M. S. Borofsky, et al. Near-infrared fluorescence imaging to facilitate super-selective arterial clamping during zero-ischaemia robotic partial nephrectomy. *BJU Int.*, 2013, 111(4): 604–610
119. T. Moroga, et al. Thoracoscopic segmentectomy with intraoperative evaluation of sentinel nodes for stage I non-small cell lung cancer. *Ann. Thorac. Cardiovasc. Surg.*, 2012, 18(2): 89–94
120. K. Gotoh, et al. A novel image-guided surgery of hepatocellular carcinoma by indocyanine green fluorescence imaging navigation. *J. Surg. Oncol.*, 2009, 100(1): 75–79
121. J. S. D. Mieog, et al. Image-guided tumor resection using real-time near-infrared fluorescence in a syngeneic rat model of primary breast cancer. *Breast Cancer Res. Treat.*, 2011, 128(3): 679–689
122. R. A. Cahill, M. Anderson, L. M. Wang, I. Lindsey, C. Cunningham, N. J. Mortensen. Near-infrared (NIR) laparoscopy for intraoperative lymphatic road-mapping and sentinel node identification during definitive surgical resection of early-stage colorectal neoplasia. *Surg. Endosc.*, 2012, 26(1): 197–204
123. Y. Liu, et al. Near-infrared fluorescence goggle system with complementary metal-oxide-semiconductor imaging sensor and see-through display. *J. Biomed. Opt.*, 2013, 18(10): 101303
124. M. A. Whitney, et al. Fluorescent peptides highlight peripheral nerves during surgery in mice. *Nat. Biotechnol.*, 2011, 29(4): 352–356
125. M. H. Park, et al. Prototype nerve-specific near-infrared fluorophores. *Theranostics*, 2014, 4(8): 823–833
126. C. Chi, et al. Intraoperative imaging-guided cancer surgery: From current fluorescence molecular imaging methods to future multi-modality imaging technology. *Theranostics*, 2014, 4(11): 1072–1084
127. M. Hutteman, et al. Clinical translation of *ex vivo* sentinel lymph node mapping for colorectal cancer using invisible near-infrared fluorescence light. *Ann. Surg. Oncol.*, 2011, 18(4): 1006–1014
128. J. S. Mieog, et al. Toward optimization of imaging system and lymphatic tracer for near-infrared fluorescent sentinel lymph node mapping in breast cancer. *Ann. Surg. Oncol.*, 2011, 18(9): 2483–2491
129. J. R. van der Vorst, et al. Near-infrared fluorescence-guided resection of colorectal liver metastases. *Cancer*, 2013, 119(18): 3411–3418
130. J. R. van der Vorst, et al. Near-infrared fluorescence sentinel lymph node mapping of the oral cavity in head and neck cancer patients. *Oral Oncol.*, 2013, 49(1): 15–19
131. L. M. A. Crane, et al. Intraoperative multispectral fluorescence imaging for the detection of the sentinel lymph node in cervical cancer: A novel concept. *Mol. Imaging Biol.*, 2011, 13(5): 1043–1049
132. M. Kijanka, et al. Rapid optical imaging of human breast tumour xenografts using anti-HER2 VHHs site-directly conjugated to IRDye 800CW for image-guided surgery. *Eur. J. Nucl. Med. Mol. Imaging*, 2013, 40(11): 1718–1729
133. R. G. Pleijhuis, et al. Near-infrared fluorescence (NIRF) imaging in breast-conserving surgery: Assessing intraoperative techniques in tissue-simulating breast phantoms. *Eur. J. Surg. Oncol.*, 2011, 37(1): 32–39
134. L. M. A. Crane, et al. Intraoperative near-infrared fluorescence imaging for sentinel lymph node detection in vulvar cancer: First clinical results. *Gynecol. Oncol.*, 2011, 120(2): 291–295
135. C. Chi, et al. Use of indocyanine green for detecting the sentinel lymph node in breast cancer patients: From preclinical evaluation to clinical validation. *PLoS ONE*, 2013, 8(12): e83927
136. N. C. Munabi, O. B. Olorunnipa, D. Goltsman, C. H. Rohde, J. A. Ascherman. The ability of intra-operative perfusion mapping with laser-assisted indocyanine green angiography to predict mastectomy flap necrosis in breast reconstruction: A prospective trial. *J. Plast. Reconstr. Aesthet. Surg.*, 2014, 67(4): 449–455
137. T. Sugie, et al. Comparison of the indocyanine green fluorescence and blue dye methods in detection of sentinel lymph nodes in early-stage breast cancer. *Ann. Surg. Oncol.*, 2013, 20(7): 2213–2218
138. J. Mohebali, L. J. Gottlieb, J. P. Agarwal. Further validation for use of the retrograde limb of the internal mammary vein in deep inferior epigastric perforator flap breast reconstruction using laser-assisted indocyanine green angiography. *J. Reconstr. Microsurg.*, 2010, 26(2): 131–135
139. A. Peloso, et al. Combined use of intraoperative ultrasound and indocyanine green fluorescence imaging to detect liver metastases from colorectal cancer. *HPB (Oxford)*, 2013, 15(12): 928–934
140. D. Gray, E. Kim, V. Cotero, P. Staudinger, S. Yazdanfar, C. T. Hehir. Compact fluorescence and white light imaging system for intraoperative visualization of nerves. In: *Proceedings of SPIE—The International Society for Optical Engineering*. Bellingham, WA: SPIE, The International Society for Optical Engineering, 2012: 8207
141. S. Keereweer, et al. Dual wavelength tumor targeting for detection of hypopharyngeal cancer using near-infrared optical imaging in an animal model. *Int. J. Cancer*, 2012, 131(7): 1633–1640
142. M. A. Whitney, et al. Fluorescent peptides highlight peripheral nerves during surgery in mice. *Nat. Biotechnol.*, 2011, 29(4): 352–356
143. M. H. Park, et al. Prototype nerve-specific near-infrared fluorophores. *Theranostics*, 2014, 4(8): 823–833
144. M. D. Jafari, et al. The use of indocyanine green fluorescence to assess anastomotic perfusion during robotic assisted laparoscopic rectal surgery. *Surg. Endosc.*, 2013, 27(8): 3003–3008
145. J. Glatz, J. Varga, P. B. Garcia-Allende, M. Koch, F. R. Greten, V. Ntziachristos. Concurrent video-rate color and near-infrared fluorescence laparoscopy. *J. Biomed. Opt.*, 2013, 18(10): 101302
146. V. Venugopal, et al. Design and characterization of an optimized simultaneous color and near-infrared fluorescence rigid endoscopic imaging system. *J. Biomed. Opt.*, 2013, 18(12): 126018
147. T. Hide, S. Yano, J. Kuratsu. Indocyanine green fluorescence endoscopy at endonasal transsphenoidal surgery for an intracavernous sinus dermoid cyst: Case report. *Neurol. Med. Chir. (Tokyo)*, 2014, 54(12): 999–1003
148. M. Plante, et al. Sentinel node mapping with indocyanine green and endoscopic near-infrared fluorescence imaging in endometrial cancer. A pilot study and review of the literature. *Gynecol. Oncol.*, 2015, 137(3): 443–447
149. Y. Pan, et al. Endoscopic molecular imaging of human bladder cancer using a CD47 antibody. *Sci. Transl. Med.*, 2014, 6(260): 260ra148
150. K. Si, R. Fiolka, M. Cui. Fluorescence imaging beyond the ballistic regime by ultrasound pulse guided digital phase conjugation. *Nat. Photonics*, 2012, 6(10): 657–661